THE JOURNAL OF PHYSICAL CHEMISTRY A

Article

pubs.acs.org/JPCA

Gas-Phase Reactions of Microsolvated Fluoride Ions: An Investigation of Different Solvents

Nicole Eyet,[†] Stephanie M. Villano,[‡] and Veronica M. Bierbaum*[,§]

[†]Saint Anselm College, 100 St. Anselm Drive #1760, Manchester, New Hampshire 03102, United States

[‡]Chemical and Biological Engineering Department, Colorado School of Mines, 125 AH, Golden, Colorado 80301, United States

[§]Department of Chemistry and Biochemistry, University of Colorado, 215 UCB Boulder, Colorado 80309-0215, United States

Supporting Information

ABSTRACT: The gas-phase reactions of $F^-(DMSO)$, $F^-(CH_3CN)$, and $F^-(C_6H_6)$ with *t*-butyl halides were investigated. Reaction rate constants, kinetic isotope effects, and product ion branching ratios were measured using the flowing afterglow selected ion flow tube technique (FA-SIFT). Additionally, the structure of $F^-(DMSO)$ was investigated both computationally and experimentally, and two stable isomers were identified. The reactions generally proceed by elimination mechanisms; however, the reaction of $F^-(C_6H_6)$ with *t*-butyl chloride occurs by a switching mechanism. These reactions are compared to previous studies of microsolvated reactions of *t*-butyl halides where the solvent molecules were polar, protic molecules.

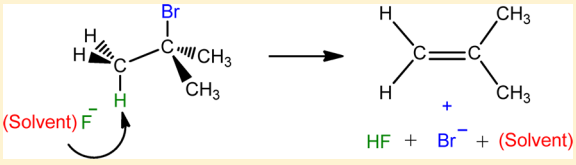

INTRODUCTION

Chemical reactions are profoundly influenced by their local environments. Reactions that occur in the condensed phase often proceed with very different rates, product branching fractions, and mechanisms than do their gas-phase analogues. The differences in reactivity for some systems in the two media raise interesting questions about the transition between the gas phase and solution. Addition of a small number of solvent molecules to gas-phase ions provides insight into this transition. Previous investigations of microsolvated ions have addressed the impact of solvation on reaction dynamics,[1−3] vibrational energy transfer,[4] charge delocalization,[5,6] and charge transfer.[7] These studies have shown that the reactivity of these ions can be dramatically influenced by the presence of a single to a few solvent molecules.[5,7−10]

The impact of microsolvation on protypical organic S_N2 reactions has been investigated. It has been shown that stepwise solvation of the nucleophile dramatically reduces the reaction rate.[8−11] Extrapolation of these rates to the bulk solvent is consistent with reaction rates measured in solution.[12] The decrease in the reaction rate is due to an increase in the barrier height upon solvation. The addition of a solvent molecule stabilizes the reactant nucleophile more strongly than the transition state. This is due to the increased charge delocalization that occurs as the reaction proceeds from the reactants to the transition state. A second observation is that the major product of these solvated S_N2 reactions is the bare leaving group ion, even though formation of the solvated ion is energetically favored.[8,9,13,14] These results are consistent with direct ab initio dynamics calculations on the reaction of $F^-(H_2O) + CH_3Cl$, which show that the product branching fractions of $Cl^- + H_2O + CH_3F$, $Cl^-(H_2O) + CH_3F$, and $Cl^- + CH_3F(H_2O)$ are dependent upon the center-of-mass collision energy and on the angle of approach.[15] In order to form solvated ionic products, the solvent molecule must cross over the CH_3F methyl group. At low collision energies (such as those in the above experiments), the solvent molecule does not have sufficient translational energy to overcome the small activation barrier associated with crossing over the neutral product.

Deuterium kinetic isotopes effects (the ratio of perprotio to perdeuterio rate constants, KIE = k_H/k_D) have been reported for the reactions of several singly solvated nucleophiles.[13,14] Deuteration of the neutral reagent and/or the solvent molecule changes the reaction rate, providing insight into the transition-state structure and hence the reaction mechanism. The origin of these effects is primarily the result of changes in vibrational frequencies as the reaction proceeds from the reactants to the transition state.[16] An inverse KIE (<1) results from the tightening of bonds in the transition state, whereas a normal KIE (>1) results from the loosening of bonds in the transition state. The reactions of $F^-(H_2O)$, $F^-(CH_3OH)$, $F^-((CH_3)_2CHOH)$, and $F^-(HF)$ with CH_3X (where X = Cl and Br) showed small to moderate inverse KIEs ($k_H/k_D < 1$) upon deuteration of the neutral reagent, which is consistent with an S_N2 mechanism.[17] Inverse KIEs were also observed upon deuteration of the solvent. These results are consistent with computations.[18,19] Hu and Truhlar investigated the effect of isotopic substitution on the reaction of $F^-(H_2O)$ with CH_3Cl using transition-state theory.[18] Their results are in excellent agreement with experiment and provide an explanation for the inverse solvent KIEs. In the transition state, the

Special Issue: Peter B. Armentrout Festschrift

Received: May 14, 2012
Revised: October 21, 2012
Published: November 12, 2012

dx.doi.org/10.1021/jp3046752 | *J. Phys. Chem. A* 2013, 117, 1136−1143

water molecule remains attached to the nucleophile via a hydrogen bond. However, because there is partial charge transfer from the nucleophile to the leaving group in the transition state, this hydrogen bond is weakened relative to that in the solvated reactant ion. As a result, the O−H bond length within the solvent molecule is shorter in the transition state, closer to that of an unbound water molecule, than that in the reactant.

Microsolvated E2 reactions have also been studied. Recently, we have reported deuterium KIEs for the reactions of several singly solvated anions with *t*-butyl halides.[20,21] Sterically bulky *t*-butyl halides are used as neutral reagents to promote an elimination mechanism. The reaction of bare fluoride ions with *t*-butyl halides has been shown to proceed through an E2 mechanism.[17] The reactions of $OH^-(H_2O)$ and $F^-(H_2O)$ with $(CH_3)_3CX$ (where X = Cl and Br) showed small normal KIEs ($k_H/k_D > 1$) upon deuteration of the neutral reagent,[21] while the reactions of $F^-(CH_3OH)$ and $F^-(C_2H_5OH)$ with $(CH_3)_3CBr$ showed moderate to large normal KIEs. These normal KIEs are indicative of an E2 mechanism.[17] In all cases, deuteration of the solvent molecule results in an inverse KIE. This observation is consistent with the inverse solvent KIEs observed for microsolvated S_N2 reactions; examination of optimized geometries of various solvated nucleophiles and their corresponding E2 transition-state structures provides a qualitatively similar explanation.[20−22] The investigated E2 reactions also tend to produce the bare leaving group ion as opposed to the solvated leaving group ion. This observation has been discussed qualitatively in terms of nonstatistical dynamics effects in the post-reaction complex.[21]

The study of these prototypical organic reactions in solution using polar aprotic and nonpolar solvents, including dimethyl sulfoxide (DMSO), benzene, and tetrahydrofuran (THF), has been used by chemists to extrapolate to gas-phase conditions.[23,24] While our previous studies have focused on singly solvated ions using polar protic solvents (water, methanol, and ethanol), this study focuses on using polar aprotic and nonpolar molecules to solvate fluoride. This paper reports the KIEs for the reactions of F^-(DMSO), $F^-(CH_3CN)$, and $F^-(C_6H_6)$ with $(CH_3)_3CX$, where X = Cl and Br. Attempts to solvate fluoride with THF and inject this anion into the reaction flow tube were unsuccessful, presumably due to the low binding energy of the cluster ion.

EXPERIMENTAL SECTION

These experiments were carried out using a flowing afterglow selected ion flow tube (FA-SIFT).[25,26] Fluoride ions are produced from electron impact on NF_3. Solvated ions are produced by introducing the desired solvent, mixed with THF, slightly downstream of the production of fluoride. This method has been shown to enhance clustering.[27] Cluster anions are mass-selected using a quadrupole mass spectrometer and injected into the reaction flow tube. Multiple collisions with helium buffer gas (~300 K, 0.5 Torr, 10^4 cm s^{-1}) ensure a thermal energy distribution of the reactant ions. A known flow of neutral reagent, measured by a calibrated volume technique, is added to the reaction flow tube through a manifold of inlets. The depletion of the reactant ions and formation of the product ions are monitored using a quadrupole mass filter coupled to an electron multiplier. Reaction rate constants are determined by varying the reaction distance and, therefore, the reaction time.

Neutral reagents were obtained from commercial sources and used without further purification. [$(CH_3)_3CBr$, 96%; $(CD_3)_3CBr$, 98% D; $(CH_3)_3CCl$, 96%; $(CD_3)_3CCl$, 99% D; NF_3, 99.7%; C_6H_6, ≥99.0%; C_6D_6, 99% D; CH_3CN, 99.8%; CD_3CN, 99.8% D; DMSO, ≥99.5%; $CD_3S(O)CD_3$, 99.9% D.] Helium buffer gas (99.995%) was purified by passage through a molecular sieve trap immersed in liquid nitrogen. Reported rate constants are the averages of at least three individual measurements, and the stated error bars reflect the standard deviations of these measurements. Errors reported for the kinetic isotope effects result from the propagation of the standard deviations. Absolute uncertainties in these rate measurements are ±20%. Systematic errors cancel in the rate constant ratio, such that the error bars for the KIEs are significantly smaller.

The product ion distributions were corrected for several factors. Correction for the bare ion, which was present as a result of collision-induced dissociation upon injection of the reactant cluster into the reaction flow tube, was necessary because its reaction with the *t*-butyl halide also formed some of the same product ions. Additionally, trace amounts (<10% of total ion signal) of $F^-(H_2O)$ were observed in the reaction flow tube as a result of background water. These complications were accounted for by monitoring all ionic reactants as a function of time and subtracting the contaminant ion contribution from the overall result. Lastly, while efforts were made to minimize mass discrimination, it was still necessary to correct the product branching ratios for the preferential detection of lower mass ions. Estimates of the mass discrimination were carried out through a series of calibration reactions, spanning the mass range of the experiment. These reactions were chosen such that a single reactant ion, when allowed to react with a carefully selected neutral reagent, formed a single ionic product.

To assist with data analysis, the structures and cluster ion bond strengths of F^-(DMSO) and $F^-(C_6D_6)$ have been measured. Bond strengths of $F^-(C_6H_6)$[28] and $F^-(CH_3CN)$[29] have been previously measured to be 64.0 and 102.5 kJ mol^{-1}, respectively. The bond strength of F^-(DMSO) was measured here using a bracketing experiment. As will be shown below, there are two stable structures of this anion, and this measurement corresponds to the higher-energy isomer. The bond strength of $F^-(C_6D_6)$ was measured in an equilibrium experiment. The bond strength of $F^-(CD_3CN)$ could not be measured in an equilibrium experiment with $F^-(CH_3CN)$ due to the observation of proton/deuteron scrambling.

THEORY

Electronic structure calculations were carried out using the Gaussian 09 program package.[30] Optimized geometries and energetics of the reactant anions were calculated using density functional theory, B3LYP/6-311++G(d,p).[31,32] The cluster binding energy of F^-(DMSO) has also been calculated using G3 calculations,[33] a composite method shown to give accurate thermodynamic information. Transition-state geometries of the reactions of $F^-(CH_3CN)$ and $F^-(C_6H_6)$ with *t*-butyl bromide and *t*-butyl chloride were calculated using the M06-2X theory. Transition states for the reactions with F^-(DMSO) could not be located. The proton affinity of F^- was also calculated at each of these levels of theory, as a check, and these values were found to be accurate to within less than 1 kcal mol^{-1}. Cartesian coordinates of all optimized geometries are provided in the Supporting Information.

dx.doi.org/10.1021/jp3046752 | J. Phys. Chem. A 2013, 117, 1136−1143

RESULTS AND DISCUSSION

Clustering Structures and Energetics. Stable structures for the solvated fluoride anions are given in Figure 1. The

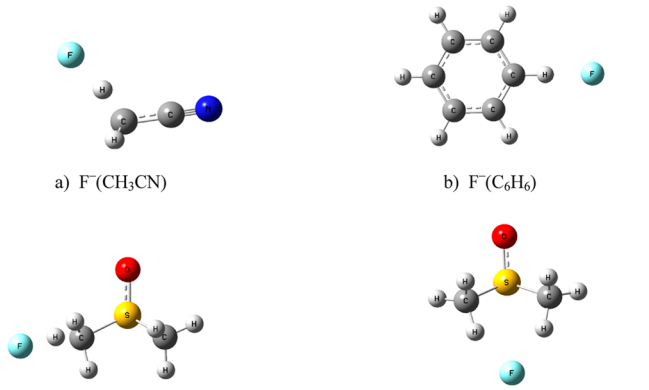

Figure 1. Calculated structures (B3LYP/6-311++G(d,p)) of solvated fluoride anions.

$F^-(CH_3CN)$[29,34] cluster (Figure 1a) and the $F^-(C_6H_6)$[28] cluster (Figure 1b) have been studied previously; our results are in good agreement with these calculations. This is the first reported study of the structures for F^-(DMSO), although the structures of Cl^-(DMSO) and Br^-(DMSO) have been computed previously.[35,36] Two stable structures of this ion are given in Figure 1c and d.

The bond strength of $F^-(C_6D_6)$ was determined by an equilibrium measurement with $F^-(C_6H_6)$. For these experiments, $F^-(C_6D_6)$ was prepared in the source region, and C_6H_6 was introduced into the reaction flow tube. The rate constant for ligand switching was measured (k_f = 6.64 × 10^{-10} cm^3 $molecule^{-1}$ s^{-1}). The reverse reaction was also studied, where $F^-(C_6H_6)$ was prepared in the source region and C_6D_6 was added to the reaction flow tube, and the rate constant for ligand switching was measured (k_r = 4.36 × 10^{-10} cm^3 $molecule^{-1}$ s^{-1}). These rate constants combine to give a $\Delta(\Delta G)$ = −1.3 kJ mol^{-1} and $\Delta(\Delta H)$ = −1.3 kJ mol^{-1}. The known binding energy (ΔH) of fluoride to benzene is 64.0 kJ mol^{-1};[28] the bond strength of $F^-(C_6D_6)$ is then 62.7 kJ mol^{-1}. No error bar is reported for the binding energy of $F^-(C_6H_6)$; therefore, no error bars are given for this determination. This result is consistent with expectations. Cluster binding strength has been observed to increase with increasing acidity of the ligand, and deuterated compounds are slightly less acidic than their hydrogenated counterparts.

Computations predict two stable structures of the F^-(DMSO) complex. In the less stable form of this complex, shown in Figure 1c, the fluoride ion interacts with a single hydrogen atom from one methyl group. In the more stable, symmetrical form of the complex, shown in Figure 1d, the fluoride ion lies below the dimethyl sulfoxide molecule and interacts with a hydrogen atom from each methyl group. It was necessary to investigate the possibility of producing both stable complexes in our ion source.

F^-(DMSO) was prepared under two sets of conditions, in the presence and the absence of THF in the ion source. Ligand switching rate constants were measured for the ion prepared by both methods. The F^-(DMSO) ion prepared in the presence of THF is completely depleted by reaction with several molecules, including methanol and ethanol. In contrast, the F^-(DMSO) ion prepared in the absence of THF shows both a reactive and unreactive component upon interaction with the same molecules. The unreactive component comprises about 10% of the total signal intensity. The reactive component is depleted at the same rate regardless of the method of preparation. Systematic variation of source conditions does not vary the ratio of the reactive to unreactive component during a single experiment. All further experiments were carried out using THF in the ion source to cleanly prepare the reactive form of F^-(DMSO).

The bond energy of the reactive F^-(DMSO) complex was determined in bracketing experiments. Rapid ligand switching reactions indicated that F^- binds more strongly to H_2O (114.6 ± 2.1 kJ mol^{-1}), to CH_3OH (123.8 ± 8.4 kJ mol^{-1}), and to C_2H_5OH (135.6 ± 2.9 kJ mol^{-1}) than to dimethyl sulfoxide. Addition of acetonitrile to the reaction flow tube results in a switching reaction that occurs at approximately 10% of the collision rate. The binding energy of $F^-(CH_3CN)$[29] is 102.5 ± 8.4 kJ mol^{-1}. Addition of deuterated benzene, its bond strength determined above, does not result in ligand switching. We therefore have determined the bond energy (ΔH) of this F^-(DMSO) isomer to be 83 ± 20 kJ mol^{-1}, between that of acetonitrile and benzene-d_6. These results are summarized in Table 1.

B3LYP/6-311++G(d,p) calculations predict a bond energy of 129.7 kJ mol^{-1} for the more stable isomer of F^-(DMSO) and 86.3 kJ mol^{-1} for the less stable isomer. G3 calculations predict a bond energy of 126.8 kJ mol^{-1} for the more stable isomer and 75.2 kJ mol^{-1} for the higher-energy isomer. The experimentally determined bond strength is in good agreement with the calculated value for the higher-energy isomer, shown in Figure 1c. The more stable isomer is likely to be the unreactive component of the F^-(DMSO) ion signal that is produced in the absence of THF in the ion source. Typically self-catalyzed rearrangement to give the lowest-energy isomer is observed in the flowing afterglow. In this case, while rearrangement to the more thermodynamically stable structure is exothermic, the

Table 1. F^-(DMSO) Cluster Switching Reactions

	reaction rate constant[a] (cm^3 $molecule^{-1}$ s^{-1})	product cluster	experimental bond energy of product cluster (kJ mol^{-1})	calculated bond energy of product cluster[b] (kJ mol^{-1})
F^-(DMSO) + C_6D_6		$F^-(C_6D_6)$	62.7[c]	67.4
F^-(DMSO) + CH_3CN	1 × 10^{-10}	$F^-(CH_3CN)$	102.5 ± 8.4	113.8
F^-(DMSO) + H_2O	8 × 10^{-10}	$F^-(H_2O)$	114.6 ± 2.1	121.8
F^-(DMSO) + CH_3OH	1 × 10^{-9}	$F^-(CH_3OH)$	123.8 ± 8.4	133.1
F^-(DMSO) + C_2H_5OH	1 × 10^{-9}	$F^-(C_2H_5OH)$	135.6 ± 2.9	136.8

[a]Measured at 298K. [b]B3LYP/6-311++G(d,p). [c]Error bars for the bond energy of $F^-(C_6H_6)$, to which this value was anchored, are unknown.

dx.doi.org/10.1021/jp3046752 | J. Phys. Chem. A 2013, 117, 1136−1143

Table 2. Bimolecular Reaction Rate Constants (k_{exp}), Reaction Efficiencies (k_{exp}/k_{col}), Kinetic Isotope Effects, and Product Ion Branching Fractions at 298 K

reaction	rate constants		KIEs (k_H/k_D)		branching fractions[e]		
	k_{exp} (10^{-10} cm^3 molecule^{-1} s^{-1})	k_{exp}/k_{col}	neutral reagent	solvent	X^-	X^-(HF/DF)	X^-(S)
$F^-(H_2O)$ + $(CH_3)_3CCl$[a]	0.878 ± 0.044	0.034	1.49 ± 0.13	0.87 ± 0.10	0.33	0.67	—
$F^-(H_2O)$ + $(CD_3)_3CCl$[a]	0.590 ± 0.041	0.023		0.85 ± 0.08	0.50	0.50	—
$F^-(D_2O)$ + $(CH_3)_3CCl$[a]	1.01 ± 0.10	0.040	1.46 ± 0.17		0.23	0.77	—
$F^-(D_2O)$ + $(CD_3)_3CCl$[a]	0.695 ± 0.045	0.028			0.46	0.54	—
$F^-(CH_3CN)$ + $(CH_3)_3CCl$[c]	3.07 ± 0.10	0.14	2.84 ± 0.20	0.53 ± 0.02	0.08	0.50	0.42
$F^-(CH_3CN)$ + $(CD_3)_3CCl$[c,d]	1.08 ± 0.07	0.05		0.48 ± 0.03	0.20	0.55	0.25
$F^-(CD_3CN)$ + $(CH_3)_3CCl$[c]	5.84 ± 0.14	0.28	2.59 ± 0.07		0.13	0.51	0.36
$F^-(CD_3CN)$ + $(CD_3)_3CCl$[c,d]	2.25 ± 0.03	0.11			0.10	0.55	0.35
$F^-(C_6H_6)$ + $(CH_3)_3CCl$[c]	10.8 ± 0.64	0.58	0.93 ± 0.07	0.93 ± 0.06	1.00	—	—
$F^-(C_6H_6)$ + $(CD_3)_3CCl$[c]	11.6 ± 0.48	0.64		0.98 ± 0.05	1.00	—	—
$F^-(C_6D_6)$ + $(CH_3)_3CCl$[c]	11.6 ± 0.25	0.63	0.97 ± 0.04		1.00	—	—
$F^-(C_6D_6)$ + $(CD_3)_3CCl$[c]	11.9 ± 0.39	0.66			1.00	—	—
$F^-(H_2O)$ + $(CH_3)_3CBr$[a]	15.0 ± 0.3	0.55	1.21 ± 0.14	0.94 ± 0.14	0.87	*f*	*f*
$F^-(H_2O)$ + $(CD_3)_3CBr$[a]	12.4 ± 1.4	0.46		0.92 ± 0.11	0.75	*f*	*f*
$F^-(D_2O)$ + $(CH_3)_3CBr$[a]	15.9 ± 0.9	0.59	1.19 ± 0.09		0.83	*f*	*f*
$F^-(D_2O)$ + $(CD_3)_3CBr$[a]	13.4 ± 0.6	0.50			0.74	*f*	*f*
$F^-(CH_3OH)$ + $(CH_3)_3CBr$[b]	6.48 ± 0.24	0.27	2.10 ± 0.11	0.73 ± 0.03	0.85	*f*	*f*
$F^-(CH_3OH)$ + $(CD_3)_3CBr$[b]	3.08 ± 0.12	0.13		0.62 ± 0.02	0.77	*f*	*f*
$F^-(CD_3OD)$ + $(CH_3)_3CBr$[b]	8.82 ± 015	0.37	1.78 ± 0.03		0.88	*f*	*f*
$F^-(CD_3OD)$ + $(CD_3)_3CBr$[b]	4.95 ± 0.05	0.21			0.83	*f*	*f*
$F^-(C_2H_5OH)$ + $(CH_3)_3CBr$[b]	3.58 ± 0.05	0.16	3.84 ± 0.33	0.63 ± 0.03	0.41	*f*	*f*
$F^-(C_2H_5OH)$ + $(CD_3)_3CBr$[b]	0.93 ± 0.08	0.042		0.44 ± 0.04	0.50	*f*	*f*
$F^-(C_2D_5OD)$ + $(CH_3)_3CBr$[b]	5.67 ± 0.04	0.26	2.70 ± 0.10		0.52	*f*	*f*
$F^-(C_2D_5OD)$ + $(CD_3)_3CBr$[b]	2.10 ± 0.08	0.098			0.50	*f*	*f*
F^-(DMSO) + $(CH_3)_3CBr$[c]	9.96 ± 0.34	0.50	1.16 ± 0.04	0.86 ± 0.04	0.52	0.48	trace
F^-(DMSO) + $(CD_3)_3CBr$[c]	8.56 ± 0.14	0.44		0.86 ± 0.05	0.32	0.68	trace
$F^-(CD_3S(O)CD_3)$ + $(CH_3)_3CBr$[c]	11.6 ± 0.42	0.60	1.16 ± 0.08		0.39	0.61	trace
$F^-(CD_3S(O)CD_3)$ + $(CD_3)_3CBr$[c]	9.95 ± 0.59	0.52			0.32	0.68	trace
$F^-(CH_3CN)$ + $(CH_3)_3CBr$[c]	15.8 ± 0.38	0.69	1.14 ± 0.03	1.07 ± 0.04	0.91	0.09	—
$F^-(CH_3CN)$ + $(CD_3)_3CBr$[c]	13.8 ± 0.09	0.61		1.02 ± 0.05	0.80	0.20	—
$F^-(CD_3CN)$ + $(CH_3)_3CBr$[c]	14.8 ± 0.44	0.65	1.09 ± 0.07		0.96	0.04	—
$F^-(CD_3CN)$ + $(CD_3)_3CBr$[c]	13.5 ± 0.72	0.61			0.86	0.14	—
$F^-(C_6H_6)$ + $(CH_3)_3CBr$[c]	13.7 ± 0.64	0.69	0.95 ± 0.06	0.99 ± 0.05	0.97	0.03	—
$F^-(C_6H_6)$ + $(CD_3)_3CBr$[c]	14.3 ± 0.48	0.74		1.01 ± 0.04	0.96	0.04	—
$F^-(C_6D_6)$ + $(CH_3)_3CBr$[c]	13.8 ± 0.25	0.72	0.97 ± 0.03		0.88	0.12	—
$F^-(C_6D_6)$ + $(CD_3)_3CBr$[c]	14.3 ± 0.39	0.75			0.94	0.06	—

[a]Reference 21 [b]Reference 20. [c]This work. [d]The reactions of $F^-(CH_3CN)$ and $F^-(CD_3CN)$ with $(CD_3)_3CCl$ also produced an association product of 2 and 0.5%, respectively. These contributions are removed from the reported bimolecular reaction rate constants. [e]Error in the branching fractions for the reactions of $F^-(CH_3CN)$ + $(CH_3)_3CCl$, $F^-(H_2O)$ + $(CH_3)_3CCl$, and $F^-(H_2O)$ + $(CH_3)_3CBr$ are ±50%; errors in the other branching fractions are ±30%. [f]Only the sum of the X^-(S) and X^-(HF/DF) cluster products is reported. The sum can be obtained from the reported bare ion branching fraction.

barrier for interconversion between the two isomers may be large.

The structures discussed above represent the most stable forms of these ions. Other alternate isomers could be envisioned due to the similar acidities of HF, CH_3CN, and DMSO, and examples of these structures are shown in the Supporting Information.

Reaction Efficiencies and Product Branching Fractions. The reactions of F^-(DMSO), $F^-(CH_3CN)$, and $F^-(C_6H_6)$ were studied with *t*-butyl chloride and/or *t*-butyl bromide. Table 2 summarizes the bimolecular reaction rate constants, reaction efficiencies, product branching fractions, and kinetic isotope effects that result from deuteration of the neutral reagent and from deuteration of the solvent. The reaction efficiency is defined as the ratio of the experimentally determined rate constant and the collisional rate constant, calculated by parametrized trajectory theory.[37] Also summarized in Table 2 are our previous results for the reactions of $F^-(H_2O)$ with *t*-butyl chloride and *t*-butyl bromide[21] and $F^-(CH_3OH)$ and $F^-(C_2H_5OH)$ with *t*-butyl bromide.[20] For the latter set of reactions, solvent KIEs were reported that result from complete deuteration of the solvent molecule and for deuteration of only the OH group. In general, the two sets of KIEs were found to be comparable, and therefore, only the results for complete deuteration of the solvent are included in Table 2 .

The microsolvated reactions investigated in Table 2 can be grouped into three categories, those that involve polar protic solvents (H_2O, CH_3OH, and C_2H_5OH), polar aprotic solvents (DMSO and CH_3CN), and nonpolar solvents (C_6H_6). With the exception of benzene, the addition of a solvent molecule reduces the reaction rate from that of the bare fluoride ion. For

dx.doi.org/10.1021/jp3046752 | J. Phys. Chem. A 2013, 117, 1136−1143

Table 3. Anion−solvent Bond Energies ($\Delta_{sol}H_{298}$) and Heats of Reaction ($\Delta_{rxn}H_{298}$) for the Various E2 Product Channels of Reactions Studied[a]

		$\Delta_{rxn}H_{298}(F^-(S) + (CH_3)_3CCl \rightarrow$ E2 products)			$\Delta_{rxn}H_{298}(F^-(S) + (CH_3)_3CBr \rightarrow$ E2 products)		
$F^-(S)$	$\Delta_{sol}H_{298}$ (kJ mol^{-1})	$\Delta_{rxn}H_{298}(1)$ (kJ mol^{-1})	$\Delta_{rxn}H_{298}(2)$ (kJ mol^{-1})	$\Delta_{rxn}H_{298}(3)$ (kJ mol^{-1})	$\Delta_{rxn}H_{298}(1)$ (kJ mol^{-1})	$\Delta_{rxn}H_{298}(2)$ (kJ mol^{-1})	$\Delta_{rxn}H_{298}(3)$ (kJ mol^{-1})
F^-		−94	n/a	n/a	−127	n/a	n/a
$F^-(H_2O)$	114.6 ± 2.1	18	−73	−44	−14	−85	−67
$F^-(CH_3OH)$	123.8 ± 8.4				−3	−74	−64
$F^-(C_2H_5OH)$	135.6 ± 2.9				8	−63	−51
$F^-(CH_3CN)$	102.5 ± 8.4	8	−83	−55	−25	−96	−85
F^-(DMSO)[b]	83.0 ± 20[b]				−40	−112	−113
$F^-(C_6H_6)$	64.0	−31	−122	−70	−65	−134	−101

[a]Reactions studied: (1) $F^-(S) + (CH_3)_3CX \rightarrow (CH_3)_2CCH_2 + HF + S + X^-$; (2) $F^-(S) + (CH_3)_3CX \rightarrow (CH_3)_2CCH_2 + S + X^-(HF)$; and (3) $F^-(S) + (CH_3)_3CX \rightarrow (CH_3)_2CCH_2 + HF + X^-(S)$. [b]Values correspond to the higher-energy isomer (see the text).

the reactions of F^- with $(CH_3)_3CBr$, the addition of a water molecule reduces the reaction efficiency by ∼25%. The addition of methanol and ethanol reduces the reaction efficiency by 62 and 77%, respectively. The reaction efficiencies are observed to decrease with increasing solvent binding energies (see Table 3). The bond energies for acetonitrile and benzene are less than those of the polar protic solvents, and the addition of these two solvent molecules does not alter the reaction efficiency. The bond energy of dimethyl sulfoxide is between that of acetonitrile and benzene. Curiously, the reaction of F^-(DMSO) with $(CH_3)_3CBr$ proceeds with an efficiency that is ∼30% lower than that for the bare fluoride ion. Similar trends are observed for the corresponding microsolvated reactions of F^- with $(CH_3)_3CCl$. In this case, addition of a water molecule to F^- significantly reduces the reaction efficiency (by ∼95%). Addition of methanol and ethanol further reduces the reaction rate below the detection limits of our instrument. The addition of an acetonitrile molecule reduces the reaction efficiency by ∼80%, while the addition of benzene reduces the reaction rate by ∼23%.

As previously mentioned, the observed decrease in the reaction efficiency upon solvation of F^- suggests that the solvent stabilizes the ionic reactant more so than it does the corresponding transition state. In general, the reaction efficiencies decrease with increasing solvent binding energies. Thus, the influence of the solvent can be deduced from the stability of the reactant ion. This indicates that the difference in binding energies between the various solvated reactant ions is not equal to the corresponding difference in binding energies in the transition state.

There are three potential reaction channels that result from an E2 reaction, shown below in reactions 1−3, where X = Cl or Br and S = solvent. Reaction 1 produces the bare leaving group ion and is energetically the least favored. In reaction 2, the leaving group is clustered to the conjugate acid, while in reaction 3, the leaving group is clustered to the solvent molecule. Due to the high binding energy of HF, reaction 2 is slightly more exothermic than reaction 3. The heats of reaction for these three channels are provided in Table 3 for each investigated reaction.

$$F^-(S) + (CH_3)_3CX \rightarrow (CH_3)_2CCH_2 + HF + S + X^- \quad (1)$$

$$F^-(S) + (CH_3)_3CX \rightarrow (CH_3)_2CCH_2 + S + X^-(HF) \quad (2)$$

$$F^-(S) + (CH_3)_3CX \rightarrow (CH_3)_2CCH_2 + HF + X^-(S) \quad (3)$$

It is important to note that because our experiment can only detect the ionic products, only reaction 2 provides direct evidence of an E2 mechanism. The ionic products from reactions 1 and 3 could also be produced from a competing S_N2 mechanism (eqs 4 and 5). However, it has previously been shown that gas-phase S_N2 reactions that involve *t*-butyl groups are significantly slower than the competing E2 mechanism, even though they are generally more exothermic and have lower reaction barriers.[17] This reduced rate is attributed to steric factors. In an S_N2 mechanism, the nucleophile attacks the reactive carbon center from the opposite side as the leaving group, and as the reaction proceeds, the substituents are inverted, resulting in a tight transition state.

$$F^-(S) + (CH_3)_3CX \rightarrow (CH_3)_3CF + S + X^- \quad (4)$$

$$F^-(S) + (CH_3)_3CX \rightarrow (CH_3)_3CF + X^-(S) \quad (5)$$

Consistent with the result of previous studies,[20,21] these reactions form a significant amount of the bare product ion (see Table 2). For several of the investigated reactions, this is the dominant reaction channel. Although the formation of the bare product ion is favored entropically, this thermodynamic contribution is small, and the enthalpic effects dominate. The tendency to form unclustered products has previously been attributed to nonstatistical dynamics in the post-reaction complex.[21] Computational studies have shown that the E2 mechanism proceeds through an anti-periplanar transition state (shown in Figure 2), where the attacking base and the leaving

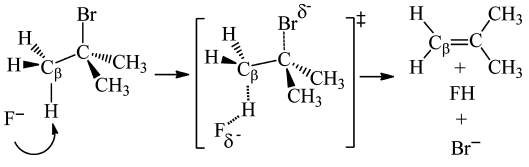

Figure 2. The E2 reaction of F^- + $(CH_3)_3CBr$.

groups are on opposite sides of the *t*-butyl group. While it could be possible for these reactions to proceed through a syn-periplanar transition state, it was previously shown that even for singly solvated systems, the syn transition state is significantly higher in energy.[20] For all transition states calculated in this work, the anti geometries were found to be significantly more energetically favorable (>35 kJ/mol) than the syn geometries.

dx.doi.org/10.1021/jp3046752 | J. Phys. Chem. A 2013, 117, 1136−1143

As a result of this anti-periplanar geometry, the bulky neutral product lies between the newly formed ionic product and the conjugate acid and solvent molecule, hindering the formation of cluster products. For the reactions that do form clustered products, the leaving group preferentially clusters to HF rather than the solvent molecule. This result reflects the higher binding energy to HF over the various solvent molecules. With the exception of the reactions of $F^-(C_6H_6)$, the cluster product branching ratio is greater for larger solvent molecules. For the reactions of $F^-(C_2H_5OH)$ and $F^-(DMSO)$ with $(CH_3)_3CBr$, the cluster branching fractions are 0.59 and 0.48, respectively. The cluster branching fractions for the corresponding reactions of $F^-(H_2O)$, $F^-(CH_3OH)$, and $F^-(CH_3CN)$ are 0.13, 0.15, and 0.09, respectively. This observation can be rationalized because larger systems have more degrees of freedom and potentially more low-frequency modes that could help facilitate vibrational coupling. In addition, the greater density of states would increase the complex lifetime. These factors suggest that the dynamics of the heavier complexes would be more statistical.

An interesting observation is that the reaction of $F^-(C_6H_6)$ with $(CH_3)_3CCl$ does not produce any cluster ion products, while the corresponding reaction with $(CH_3)_3CBr$ does produce some. In contrast, more cluster ions are formed from the reactions of $F^-(H_2O)$ and $F^-(CH_3CN)$ with *t*-butyl chloride than for the corresponding reaction with *t*-butyl bromide. This observation suggests that the reactions with *t*-butyl chloride proceed via a different mechanism than the reactions with *t*-butyl bromide. One possibility is a ligand switching mechanism followed by thermal decomposition. An analogous pathway was reported by Viggiano et al. for the reaction of $Cl^-(H_2O)$ with CH_3Br.[38] This pathway is possible due to the weak interaction of chloride and water, bound by 60 ± 20 kJ mol^{-1}, while $Cl^-(CH_3Br)$ is bound by 52.3 ± 4.2 kJ mol^{-1}; moreover, the S_N2 pathway is slightly endothermic. The $Cl^-(CH_3Br)$ product of the switching pathway, which was observed directly, also thermally decomposed to produce both Cl^- and Br^- at thermal energies, making the process initially indistinguishable from an S_N2 mechanism.

In this case, the suspected ligand switching reaction is shown in reaction 6; subsequent thermal decomposition of the $F^-((CH_3)_3CX)$ cluster produces F^- or X^-

$$F^-(C_6H_6) + (CH_3)_3CX \rightarrow F^-((CH_3)_3CX) + C_6H_6 \quad (6)$$

While this switching mechanism is unlikely for the other reactions in this study due to the high fluoride−solvent bond energy, it is possible in the case of $F^-(C_6H_6)$ because this cluster is bound by only 64.0 kJ mol^{-1}. In contrast, the $F^-((CH_3)_3CCl)$ cluster and the $F^-((CH_3)_3CBr)$ cluster are estimated to be bound by about 100 and 106 kJ mol^{-1}, respectively.

No direct evidence of the switching mechanism for $F^-(C_6H_6)$ with either *t*-butyl halide was observed. That is, a fluoride ion clustered to the alkyl halide was not detected. For the reactions of $F^-(C_6H_6)$ with *t*-butyl bromide, the elimination pathways are more exothermic than the switching pathway (ΔH_{rxn} = −42 kJ mol^{-1}); see Table 3. Additionally, minor amounts of $Br^-(HF/DF)$ are observed as products. While it is not possible to exclude the switching mechanism as a contributing pathway, the elimination mechanism is definitely occurring for $F^-(C_6H_6)$ with *t*-butyl bromide. For the corresponding reaction with *t*-butyl chloride, the switching mechanism is more exothermic (ΔH_{rxn} = −36 kJ mol^{-1}) than reaction 1 of the elimination mechanism, which produces the bare leaving group ion. In this case, because no E2 clustered products are observed to support an elimination mechanism, it is likely that a ligand switching mechanism occurs followed by thermal decomposition to produce Cl^-.

Kinetic Isotope Effects. The previously investigated reactions of F^- microsolvated with water, methanol, and ethanol showed normal KIEs (>1) upon deuteration of the *t*-butyl halide. For the reactions of F^-solvated with acetonitrile or dimethyl sulfoxide, normal neutral reagent KIEs are also observed. In contrast, the reactions of F^-solvated with benzene have slightly inverse KIEs; however, within the error bars, these values could be unity. This anomaly may reflect the high efficiencies of these reactions, or it may indicate the occurrence of an alternative mechanism, as discussed above. The observed normal KIEs for the remaining reactions are consistent with an E2 mechanism and are attributed to the elongation of the C_β−H bond in the transition state (see Figure 2) as compared to the neutral reagent. Furthermore, in each case, a hydrogen fluoride ionic cluster product ($X^-(HF)$) was observed, providing experimental evidence that these reactions proceed, at least partially, through an E2 mechanism.

In general, the normal kinetic isotope effect as a result of deuterating the neutral reagent decreases as the reaction efficiency increases, as shown in Figure 3. The reactions of

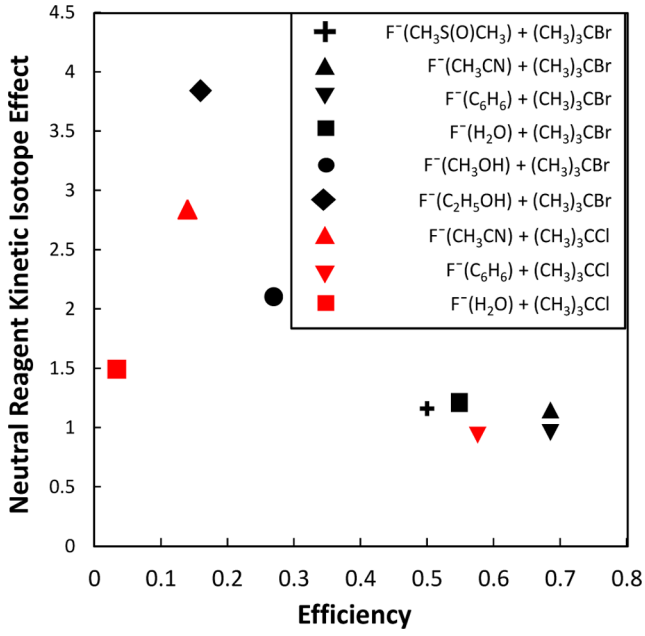

Figure 3. Neutral reagent kinetic isotope effect as a function of reaction efficiency. Kinetic isotope effects presented here are taken from this work and our previously published data. Red symbols indicate reactions with *t*-butyl chloride, and black symbols indicate reactions with *t*-butyl bromide.

$F^-(DMSO)$, $F^-(CH_3CN)$, $F^-(C_6H_6)$, and $F^-(H_2O)$ with $(CH_3)_3CBr$ proceed at similar efficiencies (~50−70%) and have comparable neutral reagent kinetic isotope effects (1.00−1.21). Because these reactions are rapid and hence are not barrier-controlled, the magnitudes of the KIEs are not expected to accurately reflect the difference in transition states. The reactions of $F^-(CH_3OH)$ and $F^-(C_2H_5OH)$ with $(CH_3)_3CBr$ are less efficient (16−27%), and the KIEs are expected to reflect the differences in transition states. These reactions display much larger KIEs. In general, the reactions with *t*-butyl

dx.doi.org/10.1021/jp3046752 | J. Phys. Chem. A 2013, 117, 1136−1143

chloride proceed less efficiently than do the analogous reactions with *t*-butyl bromide, as would be predicted by their exothermicities. The reactions of $F^-(H_2O)$ with $(CH_3)_3CCl$ proceed much less efficiently than those of $F^-(CH_3CN)$, consistent with lower exothermicities, at ~3 and ~14% efficiency, respectively. However, the isotope effects for the $F^-(CH_3CN)$ reactions are much more pronounced upon deuteration of the neutral reagent than for those of $F^-(H_2O)$ (2.84 versus 1.49). The reaction of $F^-(H_2O)$ with *t*-butyl chloride appears to be an outlier in the trend.

The solvent KIEs for the reactions of F^-solvated with water, methanol, and ethanol are inverse (<1). The solvent KIEs for the reactions of F^-solvated with acetonitrile, dimethyl sulfoxide, and benzene measured here are approximately 1 or <1. The magnitudes of these KIEs (i.e., the deviation from 1) were found to scale with the reaction efficiencies. This trend is shown by the solid symbols in Figure 4. The reactions of $F^-(CH_3CN)$ and $F^-(C_6H_6)$ with $(CH_3)_3CBr$ proceed rapidly (~70% efficiency). Because these reactions are collision-controlled, the magnitude of the KIE is not expected to accurately reflect the difference in transition states. The remaining reactions of the microsolvated fluoride ion with *t*-butyl bromide are less efficient, and these solvent KIEs are <1. The reactions with *t*-butyl chloride proceed less efficiently than do the analogous reactions with *t*-butyl bromide, and the corresponding solvent KIEs are greater in magnitude. Once again, the reaction of $F^-(H_2O)$ with *t*-butyl chloride appears to be an outlier in the trend; the reason for this is currently not clear.

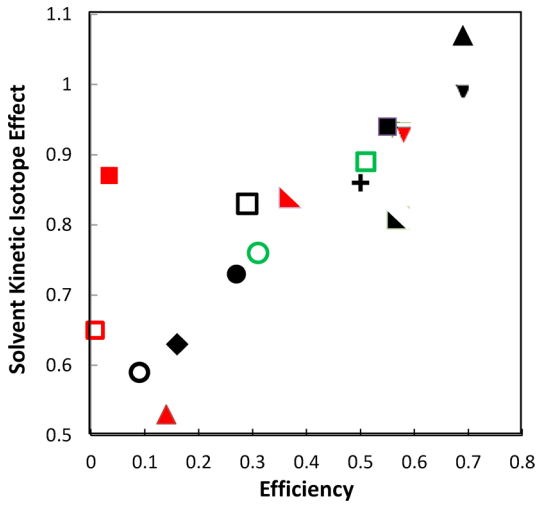

Figure 4. (Red ▲) $F^-(CH_3CN)$ + $(CH_3)_3CCl$; (black ▲) $F^-(CH_3CN)$ + $(CH_3)_3CBr$; (black **O**) $F^-(CH_3OH)$ + CH_3Br; (green **O**) $F^-(CH_3OH)$ + CH_3I; (red ■) $F^-(H_2O)$ + $(CH_3)_3CCl$; (black ■) $F^-(H_2O)$ + $(CH_3)_3CBr$; (red □) $F^-(H_2O)$ + CH_3Cl; (black □) $F^-(H_2O)$ + CH_3Br; (green □) $F^-(H_2O)$ + CH_3I; (black +) F^-(DMSO) + $(CH_3)_3CBr$; (black ●) $F^-(CH_3OH)$ + $(CH_3)_3CBr$; (red ▼) $F^-(C_6H_6)$ + $(CH_3)_3CCl$; (black ▼) $F^-(C_6H_6)$ + $(CH_3)_3CBr$; (black ♦) $F^-(C_2H_5OH)$ + $(CH_3)_3CBr$; (red right triangle) $OH^-(H_2O)$ + $(CH_3)_3CCl$; (black right triangle) OH^- (H_2O) + $(CH_3)_3CBr$. Solvent kinetic isotope effect as a function of reaction efficiency. Kinetic isotope effects presented here are taken from this work and previously published data (from ref 13, $F^-(CH_3OH)$ + CH_3Br, $k = 1.63 \times 10^{-10}$ eff = 0.09, SKIE = 0.59; $F^-(CH_3OH)$ + CH_3I, $k = 5.20 \times 10^{-10}$, eff = 0.31, SKIE = 0.76; from ref 14, $F^-(H_2O)$ + CH_3Cl, $k = 0.149 \times 10^{-10}$, eff = 0.008, SKIE = 0.65; $F^-(H_2O)$ + CH_3Br, $k = 4.97 \times 10^{-10}$, eff = 0.29, SKIE = 0.83; $F^-(H_2O)$ + CH_3I, $k = 8.64 \times 10^{-10}$, eff = 0.51, SKIE = 0.89; from ref 21, $OH^-(H_2O)$ + $(CH_3)_3CCl$, $k = 9.20 \times 10^{-10}$, eff = 0.37, SKIE = 0.84 ; $OH^-(H_2O)$ + $(CH_3)_3CBr$, $k = 1.60 \times 10^{-9}$, eff = 0.57, SKIE = 0.81). Open symbols represent previously studied reactions with methyl halides; closed symbols represent reactions with a *t*-butyl halide. Red symbols indicate reactions with an alkyl chloride, black symbols those with an alkyl bromide, and green symbols those with an alkyl iodide.

Inverse solvent KIEs are also observed for microsolvated S_N2 reactions.[13,19] For comparison, several microsolvated S_N2 solvent KIEs are included as open symbols in Figure 4. The two sets of data correlate well together. For both reaction types, the inverse effects are attributed to a decrease in bond length within the solvent molecule in the transition state, relative to those bonds in the reactant ion. The similar trends suggest that for reactions with similar efficiencies, the change in the solvent−ion hydrogen bond is similar regardless of the reaction mechanism. This implies that the amount of charge transfer between the attacking ion and the leaving group ion is similar for both mechanisms.

For the reactions of $F^-(CH_3OH)$ and $F^-(C_2H_5OH)$ with *t*-butyl bromide, it was observed that deviation from separability occurs.[13,20] That is, the isotope effect as a result of deuterating the *t*-butyl halide is not independent of the isotopic substitution of the alcohol solvent. This was attributed primarily to the size of the solvent molecule; larger solvent molecules can interact with the neutral reactant while remaining attached to the fluoride ion. All of the isotope effects measured here, for the polar aprotic and nonpolar solvents, are found to be separable within error bars. This result can be determined from eq 7 for the reaction of $F^-(CH_3CN)$ with $(CH_3)_3CBr$ and analogous equations for the other reactions.

$$\begin{aligned} \mathrm{KIE} &= \frac{k[F^-(CH_3CN) + (CH_3)_3CBr]}{k[F^-(CD_3CN) + (CD_3)_3CBr]} \\ &\approx \frac{k[F^-(CH_3CN) + (CH_3)_3CBr]}{k[F^-(CH_3CN) + (CD_3)_3CBr]} \\ &\times \frac{k[F^-(CH_3CN) + (CH_3)_3CBr]}{k[F^-(CD_3CN) + (CH_3)_3CBr]} \end{aligned} \quad (7)$$

While this result may seem counterintuitive because DMSO is a more bulky solvent than C_2H_5OH, the structure of the solvated anion must be considered. When the $F^-(C_2H_5OH)$ ion attacks the *t*-butyl halide, most likely in an anti-elimination transition state, the unbound end of the flexible ethanol molecule can interact with the *t*-butyl halide. For F^-(DMSO) (Figure 1c), the structure around the carbonyl group makes the solvent molecule more rigid, preventing the far end of the solvent molecule from interacting with the *t*-butyl group. Therefore, the size of the solvent molecule alone does not determine whether the isotope effects are completely separable; instead, the complete geometry of the solvated anion must be considered.

In general, the measured kinetic isotope effects are separable and correlate with reaction efficiency. We have examined whether the neutral reagent or the solvent kinetic isotope effects can be explained by the nature of the solvent molecule. Unfortunately, none of these individual properties (including solvent polarizability, dielectric constant, dipole moment, anion bond strength, anion polarizability, and anion dipole moment) appear to simply correlate with the general reaction trends and kinetic isotope effects.

dx.doi.org/10.1021/jp3046752 | J. Phys. Chem. A 2013, 117, 1136−1143

CONCLUSIONS

The reactions of fluoride ions solvated by dimethyl sulfoxide, acetonitrile, and benzene all proceed through elimination mechanisms with *t*-butyl bromide at rates that approach their collision-controlled limits (50−75% efficient). The reaction of benzene-solvated fluoride with *t*-butyl chloride likely proceeds through a ligand switching mechanism followed by thermal decomposition. The reaction of acetonitrile-solvated fluoride with *t*-butyl chloride proceeds through an elimination mechanism at rates well below the collision controlled limit (∼14% efficient). This reaction shows normal kinetic isotope effects upon deuteration of the neutral reagent and inverse kinetic isotope effects as a result of deuterating the solvent molecule. All of the isotope effects measured here were found to be separable. Solvent kinetic isotope effects were compared with previously measured substitution and elimination data for microsolvated ions. While the kinetic isotope effects measured here, and previously, are shown to scale with reaction efficiency, they do not appear to correlate with any single characteristic property of the solvent.

ASSOCIATED CONTENT

Supporting Information

Coordinates and energies of calculations described in the theoretical methods. Higher energy isomers of the fluoride ions solvated by dimethylsulfoxide and acetonitrile. This material is available free of charge via the Internet at http://pubs.acs.org.

AUTHOR INFORMATION

Corresponding Author

*E-mail: Veronica.Bierbaum@colorado.edu.

Notes

The authors declare no competing financial interest.

ACKNOWLEDGMENTS

The authors thank Professor Charles H. DePuy for valuable discussions and the reviewers for their helpful comments. We gratefully acknowledge support from the National Science Foundation through Grant CHE-1012321 and through TeraGrid resources provided by NCSA.[39]

REFERENCES

(1) Greenblatt, B. J.; Zanni, M. T.; Neumark, D. M. *Science* **1997**, *276*, 1675−1678.
(2) Kim, N. J.; Paik, D. H.; Zewail, A. H. *J. Chem. Phys.* **2003**, *118*, 6930−6940.
(3) Papanikolas, J. M.; Vorsa, V.; Nadal, M. E.; Campagnola, P. J.; Buchenau, H. K.; Lineberger, W. C. *J. Chem. Phys.* **1993**, *99*, 8733−8750.
(4) Davis, A. V.; Wester, R.; Bragg, A. E.; Neumark, D. M. *J. Chem. Phys.* **2002**, *117*, 4282−4292.
(5) Relph, R. A.; Guasco, T. L.; Elliott, B. M.; Kamrath, M. Z.; McCoy, A. B.; Steele, R. P.; Schofield, D. P.; Jordan, K. D.; Viggiano, A. A.; Ferguson, E. E.; et al. *Science* **2010**, *327*, 308−312.
(6) Szpunar, D. E.; Kautzman, K. E.; Faulhaber, A. E.; Neumark, D. M. *J. Chem. Phys.* **2006**, *124*, 054318−054326.
(7) Sheps, L.; Miller, E. M.; Horvath, S.; Thompson, M. A.; Parson, R.; McCoy, A. B.; Lineberger, W. C. *Science* **2010**, *328*, 220−224.
(8) Bohme, D. K.; Mackay, G. I. *J. Am. Chem. Soc.* **1981**, *103*, 978−979.
(9) Viggiano, A. A.; Arnold, S. T.; Morris, R. A. *Int. Rev. Phys. Chem.* **1998**, *17*, 147−184.
(10) Viggiano, A. A.; Arnold, S. T.; Morris, R. A.; Ahrens, A. F.; Hierl, P. M. *J. Phys. Chem.* **1996**, *100*, 14397−14402.
(11) Bohme, D. K.; Raskit, A. B. *Can. J. Chem.* **1985**, *63*, 3007−3011.
(12) Bogdanov, B.; McMahon, T. B. *Int. J. Mass. Spectrom.* **2005**, *241*, 205−223.
(13) Kato, S.; Hacaloglu, J.; Davico, G. E.; DePuy, C. H.; Bierbaum, V. M. *J. Phys. Chem. A* **2004**, *108*, 9887−9891.
(14) O'Hair, R. A. J.; Davico, G. E.; Hacaloglu, J.; Dang, T. T.; DePuy, C. H.; Bierbaum, V. M. *J. Am. Chem. Soc.* **1994**, *116*, 3609−3610.
(15) Tachikawa, H. *J. Phys. Chem. A* **2001**, *105*, 1260−1266.
(16) Poirier, R. A.; Wang, Y. L.; Westaway, K. C. *J. Am. Chem. Soc.* **1994**, *116*, 2526−2533.
(17) DePuy, C. H.; Gronert, S.; Mullin, A.; Bierbaum, V. M. *J. Am. Chem. Soc.* **1990**, *112*, 8650−8655.
(18) Hu, W.-P.; Truhlar, D. G. *J. Am. Chem. Soc.* **1994**, *116*, 7797−7800.
(19) Davico, G. E. *J. Phys. Chem. A* **2006**, *110*, 13112−13121.
(20) Eyet, N.; Villano, S. M.; Bierbaum, V. M. *J. Am. Soc. Mass Spectrom.* **2008**, *19*, 1296−1302.
(21) Eyet, N.; Villano, S. M.; Kato, S.; Bierbaum, V. M. *J. Am. Soc. Mass Spectrom.* **2007**, *18*, 1046−1051.
(22) Wu, Y.-R.; Hu, W.-P. *J. Am. Chem. Soc.* **1999**, *121*, 10168−10177.
(23) Fang, Y.-r.; Gao, Y.; Ryberg, P.; Eriksson, J.; Kołodziejska-Huben, M.; Dybała-Defratyka, A.; Madhavan, S.; Danielsson, R.; Paneth, P.; Matsson, O.; et al. *Chem.—Eur. J.* **2003**, *9*, 2696−2709.
(24) Fang, Y.-r.; MacMillar, S.; Eriksson, J.; Kołodziejska-Huben, M.; Dybała-Defratyka, A.; Paneth, P.; Matsson, O.; Westaway, K. C. *J. Org. Chem.* **2006**, *71*, 4742−4747.
(25) Bierbaum, V. M. Flow Tubes. In *Encyclopedia of Mass Spectrometry*; Gross, M. L., Caprioli, R., Eds.; Elsevier: San Diego, CA, 2003; Vol. *1*.
(26) Van Doren, J. M.; Barlow, S. E.; DePuy, C. H.; Bierbaum, V. M. *Int. J. Mass. Spectrom. Ion Processes* **1987**, *81*, 85−100.
(27) Bickelhaupt, F. M.; de Koning, L. J.; Nibbering, N. M. M. *Tetrahedron* **1993**, *49*, 2077−2092.
(28) Hiraoka, K.; Mizuse, S.; Yamabe, S. *J. Chem. Phys.* **1987**, *86*, 4102−4105.
(29) Hiraoka, K.; Mizuse, S.; Yamabe, S. *J. Phys. Chem.* **1988**, *92*, 3943−3952.
(30) Frisch, M. J.; Trucks, G. W.; Schlegel, H. B.; Scuseria, G. E.; Robb, M. A.; Cheeseman, J. R.; Scalmani, G.; Barone, V.; Mennucci, B.; Petersson, G. A. et al. *Gaussian 09*, revision B.01; Gaussian, Inc.: Wallingford, CT, 2012.
(31) Becke, A. D. *J. Chem. Phys.* **1993**, *98*, 5648−5652.
(32) Lee, C.; Yang, W. T.; Parr, R. G. *Phys. Rev. B* **1988**, *37*, 785−789.
(33) Curtiss, L. A.; Raghavachari, K.; Redfern, P. C.; Rassolov, V.; Pople, J. A. *J. Chem. Phys.* **1998**, *109*, 7764−7776.
(34) Yamabe, S.; Hirao, K. *Chem. Phys. Lett.* **1981**, *84*, 598−603.
(35) Magnera, T. F.; Caldwell, G.; Sunner, J.; Ikuta, S.; Kebarle, P. *J. Am. Chem. Soc.* **1984**, *106*, 6140−6146.
(36) Burk, P.; Molder, U.; Koppel, I.; Rummel, A.; Trummal, A. *J. Phys. Chem.* **1996**, *100*, 16137−16140.
(37) Su, T.; Chesnavich, W. J. *J. Chem. Phys.* **1982**, *76*, 5183−5185.
(38) Viggiano, A. A.; Morris, R. A.; Paschkewitz, J. S.; Paulson, J. F. *J. Am. Chem. Soc.* **1992**, *114*, 10477−10482.
(39) Catlett, C. In *TeraGrid: Analysis of Organization, System Architecture, and Middleware Enabling New Types of Applications*; Grandinetti, L., Ed.; IOS Press: Amsterdam, The Netherlands, 2007.